ACS OMEGA

http://pubs.acs.org/journal/acsodf

Article

Functionalized Boron Nanoparticles as Potential Promising Antimalarial Agents

Yinghuai Zhu,* Parichat Prommana, Narayan S. Hosmane, Paolo Coghi, Chairat Uthaipibull,* and Yingjun Zhang

Cite This: *ACS Omega* 2022, 7, 5864−5869

Read Online

ACCESS | Metrics & More | Article Recommendations | Supporting Information

ABSTRACT: Boron nanoparticles (BNPs), functionalized with hydroxyl groups, were synthesized *in situ* by a cascade process, followed by bromination and hydrolyzation reactions. These functionalized BNPs, ($B_m(OH)_n$), were characterized using ^1H and ^{11}B NMR spectra, Fourier-transform infrared (FT-IR) spectroscopy, inductively coupled plasma-optical emission spectroscopy (ICP-OES), transmission electron microscopy (TEM), dynamic light scattering (DLS), and X-ray photoelectron spectroscopy (XPS) methods. These nanoparticles were also evaluated *in vitro* for their antimalarial activity against *Plasmodium falciparum* (3D7 strain) with an IC_{50} value of 0.0021 μM and showed low toxicity to Uppsala 87 malignant glioma (U87MG) cell lines, malignant melanoma A375 cell lines, KB human oral cancer cell lines, rat cortical neuron cell lines, and rat fibroblast-like synoviocyte (FLS) cell lines.

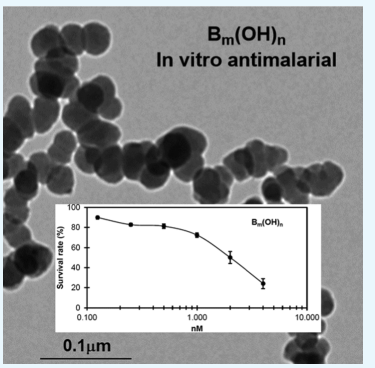

1. INTRODUCTION

Malaria is one of the world's deadliest diseases and spread through the bites of infected mosquitoes Anopheles.[1] Five species of *Plasmodium* parasites, *P. falciparum*, *P. malariae*, *P. vivax*, *P. ovale*, and *Pheidole knowlesi*, are often found to infect humans. The yearly cumulative number of cases reported globally is nearly 230 million, and the number of cumulative deaths has reached 409 000.[2] The most vulnerable group affected by malaria is children aged under 5 years; they accounted for 67% of all malaria deaths worldwide in 2019. Chloroquine (CQ, Figure 1) was one of the most widely used

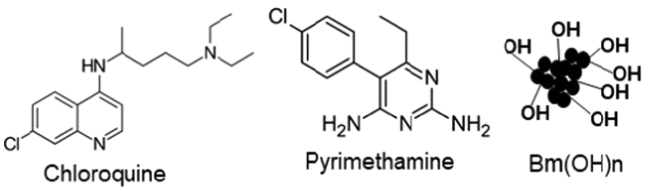

Figure 1. Structures of antimalarial drugs.

antimalarial drugs, which has now been partially substituted by artemisinin (ART) and its synthetic derivatives.[3] Pyrimethamine (Figure 1) is another recognized diaminopyrimidine-based antimalarial drug, an inhibitor of malarial dihydrofolate reductase (DHFR).[4] Although these antimalarial drugs are widely used in clinics, drug resistance is becoming a very concerning issue according to a report of the World Health Organization (WHO).[5] In such a situation, a parasite strain that may cause malarial infections can still survive and/or multiply despite an antimalarial drug being normally administrated and absorbed. To prevent the attack of drug-resistant parasites, WHO has recommended the combination of different types of antimalarial drugs; for example, combining artemisinins with one or more antimalarial drugs such as lumefantrine, amodiaquine, and piperaquine as artemisinin combination therapy (ACT).[6] Reports of decreased efficacy, reduced parasite clearance time in the case of ACT treatment, and widespread resistance by *Plasmodium* parasites suggest the need for a new search for novel pharmaceutical interventions for malaria.[7]

Boron-based drugs represent a new class of molecules that have been found to exhibit attractive properties and activities against a number of protozoans causative of neglected tropical diseases and cryptosporidiosis and toxoplasmosis.[8,9] In the last few decades, numerous bioactive molecules and molecular tools containing boron atoms have been developed.[8] A few organoboron compounds were approved by the FDA for clinical treatments. For example, 5-fluorobenzoxaborole was approved in 2014 for the treatment of onychomycosis;[10] crisaborole was also approved by the FDA in 2016 for the clinical treatment of mild-to-moderate atopic dermatitis.[11] For its molecular mechanism, a boron-containing drug generally

Received: October 26, 2021
Accepted: January 19, 2022
Published: February 9, 2022

has a hydroxyl group connecting directly to the boron center to form a borate.[8] The resulting boronate is reported to interact with a target protein through covalent bonding with nucleophilic entities (such as hydroxyl and amine groups of enzymes) to form a stable bond with the enzymes, thereby leading to their reversible inhibition. Also, it has been found that the boronic acid species may react with peptides to form the corresponding peptidyl boronates/boronic acids, which have various biological activities.[12,13] On the other hand, nanomaterials have been employed as drug carriers in antimalarial therapies and have shown high capacity in delivering sufficient drugs at local doses, thus avoiding drug resistance development.[14,15] Nanomaterials are applicable in varying stages of malarial parasites to enhance the drug efficacy in both human and mosquito hosts.[14,15] In this study, we combined the inherent advantages of both boric acid-based drug and nanomaterial and synthesized hydroxyl group-functionalized boron nanoparticles ($B_m(OH)_n$) and evaluated its cytotoxicity and antimalarial activity.

2. RESULTS AND DISCUSSION

2.1. Compounds. While hydroxyl-functionalized boron nanoparticles ($B_m(OH)_n$) were synthesized by a straightforward route, the precursor, boron nanoparticles (BNPs), was prepared according to a literature method.[16] In brief, the BNPs were prepared by the reduction reaction of $B(NCO)_3$ in solution by pure hydrogen gas. Boron nanoparticles reacting with bromine in carbon disulfide (CS_2) afforded bromine-functionalized boron nanoparticles. The resulting nanoparticles underwent a hydrolysis reaction in a basic aqueous solution and produced hydroxyl-functionalized boron nanoparticles, $B_m(OH)_n$. Compound $B_m(OH)_n$ was characterized using ICP-OES, NMR spectra, and FT-IR spectra. No resonances of organic functional groups were observed in the ^{1}H NMR spectra of $B_m(OH)_n$ as shown in Figure 2b. The results were consistent with its molecular structure. In the ^{11}B NMR (^{1}H-coupled) spectra of $B_m(OH)_n$ (Figure 2c), a very broad peak at a chemical shift (δ) of 30.15 ppm was observed for the ^{11}B resonances of the B(OH) moiety. The results are consistent with the chemical shift of ^{11}B atom in the molecule of diboronic acid, $B_2(OH)_4$.[17] In the FT-IR spectra (Figure 2d), $B_m(OH)_n$ showed main peaks at 3447, 1409, and 1080 cm^{-1}, which could be attributed to the stretching absorptions of the O−H and B−O bonds. Boron analysis was carried out using ICP-OES to further characterize the new product, and the results showed that the boron concentration was 98.77%, the ratio of m/n was 126.32, and the average molecular weight was 1.126×10^7 (g/mol). $B_m(OH)_n$ was also analyzed using TEM (Figure 3a). The TEM image showed that the nanoparticles have a relatively narrow range of around 14−36 nm in particle size distribution with an average diameter of ∼21 nm (Figure 3b). The particle size was further analyzed by the dynamic light scattering (DLS) method in aqueous solution as shown in Figure 3c. The average DLS size of the particles was about 21 nm. The results are consistent with those of the TEM analysis. XPS analysis was conducted for $B_m(OH)_n$ to prove the presence of elements and the chemical environment at the particle surface. High-resolution B 1s XPS spectra are presented in Figure 3d. Boron was observed in two oxidation states, where the peak at 187.1 eV corresponds to the elemental boron (B^0) and the peak at 193.2 eV is due to oxidation of boron (B^{3+}). These results are consistent with the literature report.[18] The survey scans confirm the presence of

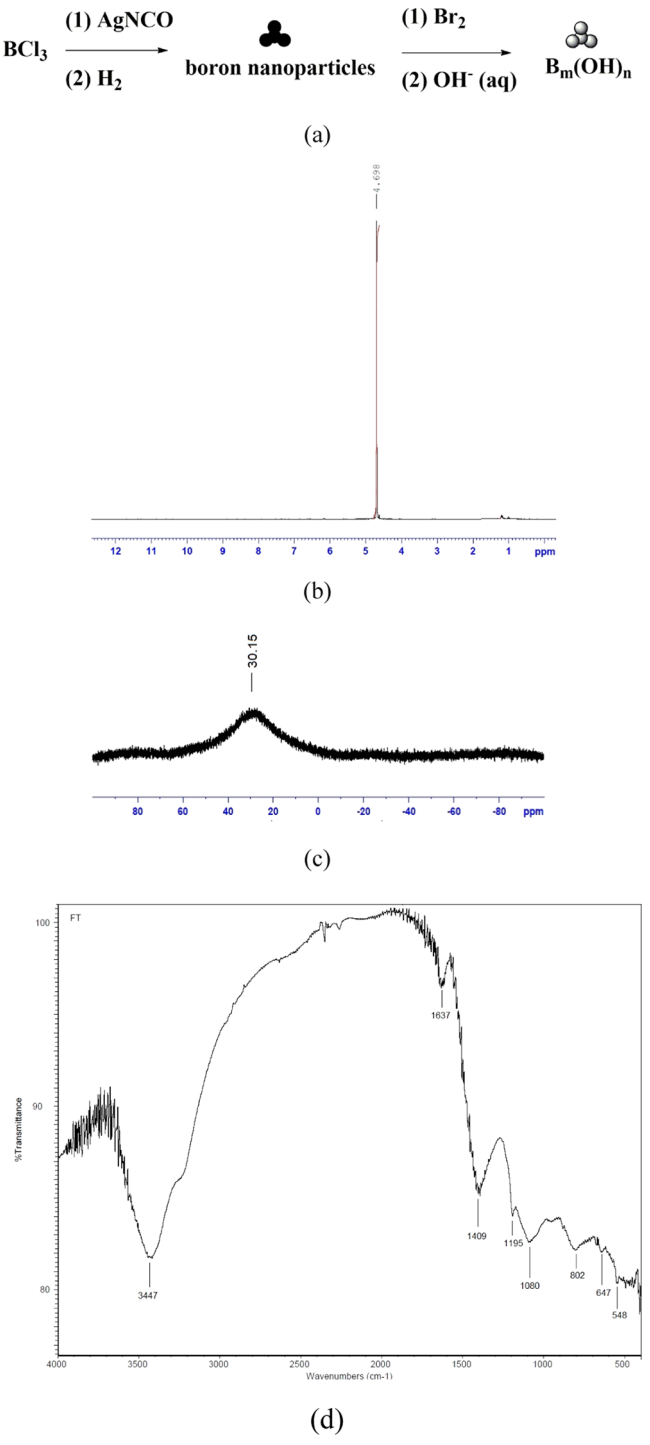

Figure 2. Synthetic route (a), ^{1}H NMR spectra (b), ^{11}B NMR spectra (c), and FT-IR spectra (d) of hydroxyl-functionalized boron nanoparticles ($B_m(OH)_n$).

boron and oxygen (Figure S1). $B_m(OH)_n$ is a deep dark-brown powder and homogeneously suspensive in deionized water and remains intact for more than 2 weeks. The unique characteristics could benefit its pharmaceutical application. The aqueous solution of $B_m(OH)_n$ is much more stable than the solutions in diethyl ether and ethyl acetate, since precipitation occurs quickly after a few hours in the latter solutions. The real mechanism of the formation of $B_m(OH)_n$ remains unclear at the current stage. Nevertheless, it is recognized that the nanoparticles demonstrate intensified behavior and properties

https://doi.org/10.1021/acsomega.1c05888
ACS Omega 2022, 7, 5864−5869

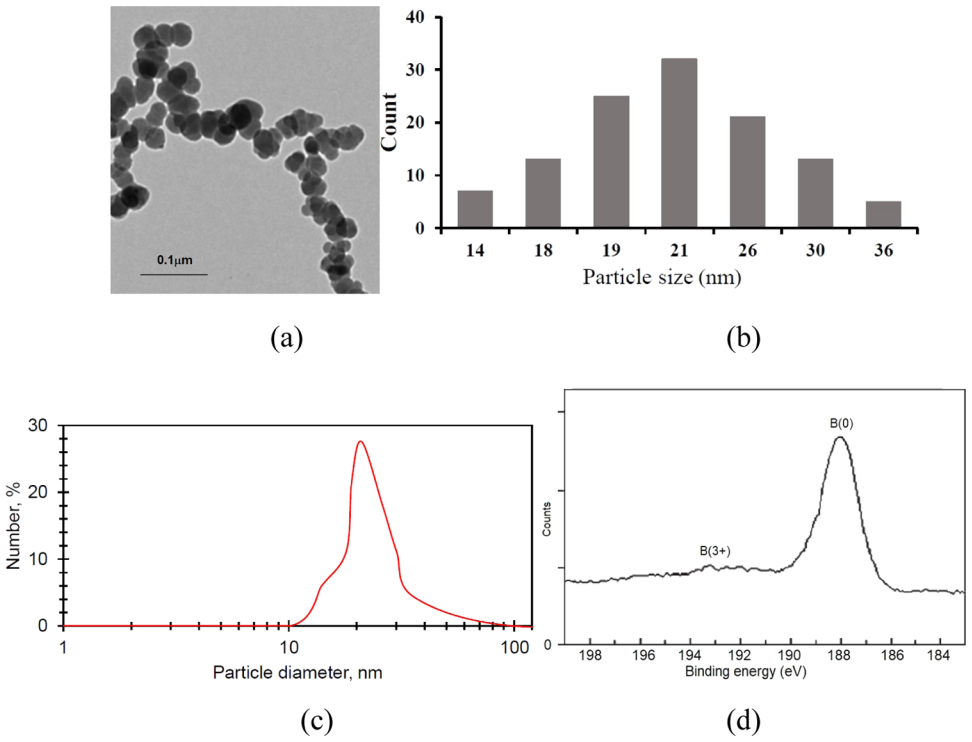

Figure 3. TEM image (a), particle size distribution histograms (b), DLS-based particle size distribution (c), and high-resolution XPS spectra of B 1s (d) of hydroxyl boron nanoparticles ($B_m(OH)_n$).

of their bulky forms due to a significant increase in the surface area. This phenomenon has also been observed for boron nanoparticles. It has been proven that the reactivity of inorganic nanoparticles increases as the particle size falls to the nanoscale.[19] Therefore, it is reasonably expected that the boron nanoparticles are more reactive than bulky boron to produce $B_m(OH)_n$.

2.2. Cytotoxicity and Boron Uptake Assay. The *in vitro* cytotoxicity of the hydroxyl-functionalized boron nanoparticles $B_m(OH)_n$ for the Uppsala 87 malignant glioma (U87MG) cell lines, malignant melanoma A375 cell lines, KB human oral cancer cell lines, rat cortical neuron cell lines, and rat fibroblast-like synoviocyte (FLS) cell lines was determined. As shown in Figure 4, the IC_{50} values of $B_m(OH)_n$ were greater than 1000 μM for all of the examined cell lines. The FLS and U87MG cells were used to examine the boron uptake of $B_m(OH)_n$. The boron concentration was determined using ICP-OES. The analytical results showed that boron uptakes for the nanoparticles of $B_m(OH)_n$ in U87MG and FLS cell lines were 201.53 and 147.64 μg boron/10^7 cells, respectively. The results strongly suggest that the nanoparticles possess low cytotoxicity for these cell lines. The results also suggest that the functionalized nanoparticles possess membrane-permeable potential by an endocytic pathway.

2.3. *In Vitro P. falciparum* Growth Inhibition Assay. The asexual 3D7 strain of *P. falciparum* parasites was used to evaluate the antimalarial capacity of the hydroxyl-functionalized boron nanoparticles ($B_m(OH)_n$). As shown in Figure 5, the IC_{50} antimalarial activity of ($B_m(OH)_n$) (BN1) was 2.11 ± 0.34 nM, while standard antimalarial drugs used as positive antimalarial controls, pyrimethamine (PYR) and chloroquine (CQ), showed IC_{50} values of 0.09 ± 0.004 μM and 14.66 ± 0.22 nM, respectively. Although the real mechanism of $B_m(OH)_n$ inhibiting *P. falciparum in vitro* is unknown at the

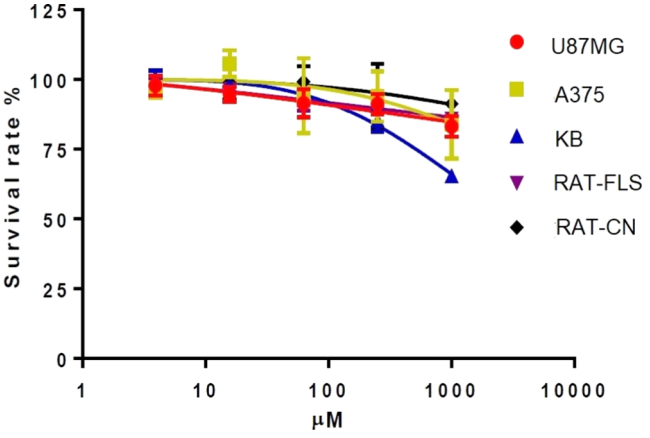

Figure 4. IC_{50} values of hydroxyl boron nanoparticles ($B_m(OH)_n$) for the Uppsala 87 malignant glioma (U87MG) cell lines, malignant melanoma A375 cell lines (A375), KB human oral cancer cell lines (KB), rat fibroblast-like synoviocyte (RAT-FLS) cell lines, and rat cortical neuron (RAT-CN) cell lines.

current stage, the following possibilities might inhibit the growth of the intracellular malaria parasite, and they cannot be excluded. (1) $B_m(OH)_n$ targets the merozoites during the period of their release from one cell and invasion of another, (2) $B_m(OH)_n$ inhibits parasite invasion, and (3) $B_m(OH)_n$ enters the parasitophorous vacuole during the endocytosis invasion process and, subsequently, inhibits the growth of the parasite.[20] However, it has been reported that there are many alterations for the malarial parasite-invaded red blood cells, such as modification in the membrane cytoskeleton, deformability, and changes in the permeability.[20,21] Accordingly, it is reasonable to propose that nanoparticles $B_m(OH)_n$ would be able to penetrate the leaky membrane of the host red

https://doi.org/10.1021/acsomega.1c05888
ACS Omega 2022, 7, 5864−5869

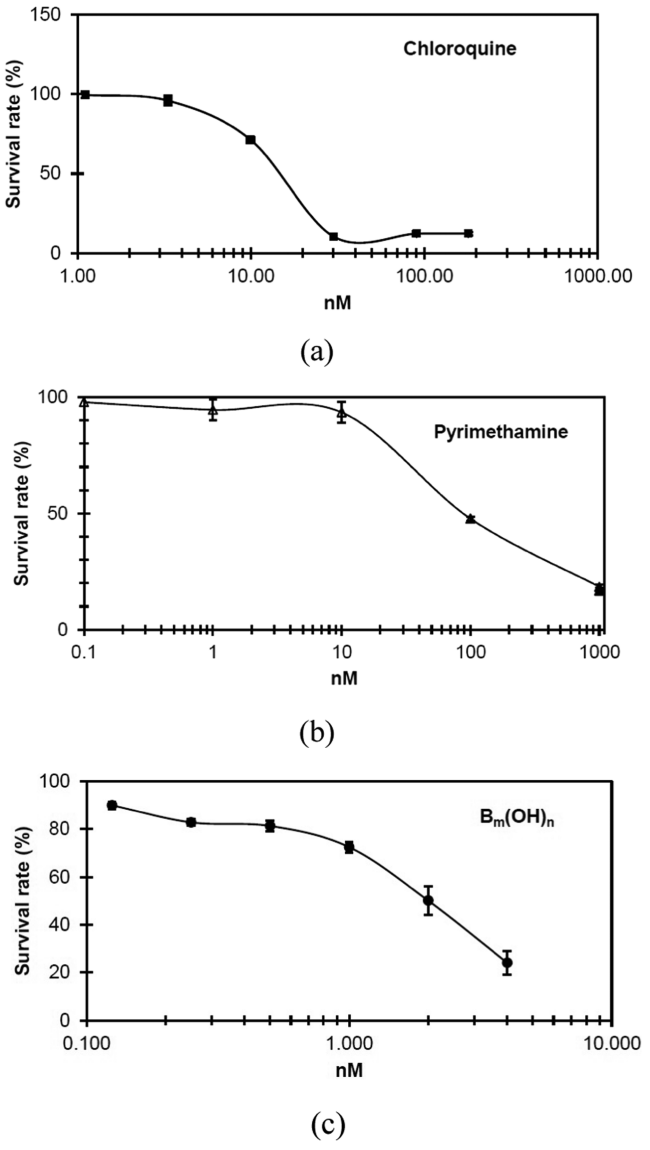

Figure 5. Antimalarial activities of chloroquine (a), pyrimethamine (b), and hydroxyl-functionalized boron nanoparticles ($B_m(OH)_n$) (c).

blood cells and, therefore, demonstrate their enhanced antimalarial efficacy as shown in our study. The interaction mechanism between $B_m(OH)_n$ and the receptor proteins is not yet known at the current stage of investigation. Nevertheless, it has been well recognized that boron-containing drugs generally have an electrophilic center of boron due to the empty p orbital in the boron element.[8] These drugs always appear as strong Lewis acids and tend to accept lone-pair electrons from a nucleophile such as enzyme proteins. After accepting a lone pair of electrons, the boron atom hybrid changes from an sp^2 hybrid with trigonal conformation to an sp^3 hybrid that has tetrahedral conformation. Therefore, it is reasonable to adopt the above-known mechanism of borate drugs for the compound in the current study, $B_m(OH)_n$. In addition, there are conflicting results being reported regarding the specific uptake of macromolecules by the malaria-infected erythrocyte, evidenced by both the fluorescence and electron micrographs.[21] Therefore, more bioassessments, such as *in vivo* examination, are necessary for compound $B_m(OH)_n$ to further confirm its antimalarial efficacy and also understand the interaction mechanism. Due to their unique electronic and structural properties, boron compounds are expected to lead the new generation of antibiotic drugs and overcome the growing problems of bacterial drug resistance.[8,22,23] Therefore, it is expected that compound $B_m(OH)_n$ may reasonably alleviate the drug resistance issue in malarial treatment if it could be used in clinical trials.

3. CONCLUSIONS

In conclusion, the newly synthesized and fully characterized hydroxyl-functionalized boron nanoparticles, $B_m(OH)_n$, possess low cytotoxicity and cell membrane permeability. They also demonstrate *in vitro* high antimalarial efficacy in comparison with current clinical antimalarial drugs, such as pyrimethamine and chloroquine. Thus, boron nanoparticles appear to have a high potential for the development of next-generation antimalarial drugs and the development of nanotechnology-based medicines against malaria. The compound, prepared in this study, warrants further investigations, including *in vivo* bioassessments, which are currently ongoing in our laboratories.

4. MATERIALS AND METHODS

4.1. Materials. All reactions were carried out under an argon atmosphere using standard Schlenk-line techniques or in a glovebox. Solvents were dried according to the established methods and freshly distilled before use.[24] Bromine, deuterated solvents, and other chemicals were purchased from Sigma-Aldrich Pte. Ltd. Boron nanoparticles were prepared according to the procedure reported in the literature.[16] The ^1H- and ^{11}B NMR spectra were recorded on a Bruker Fourier-Transform multinuclear NMR spectrometer at 200, 64.2, and 50.3 MHz relative to external Me_4Si (TMS) and $BF_3{\cdot}OEt_2$ standards, respectively. All NMR spectra were recorded at ambient temperature. The FT-IR spectra were measured using an IRTracer-100 Shimadzu spectrophotometer with KBr pellets. The FT-IR multiplicities are reported as (peak shape, strength) s = singlet, vs = very strong, m = medium, and w = weak. Inductively coupled plasma-optical emission spectroscopy (ICP-OES) analysis was performed using a VISTA-MPX, CCD Simultaneous ICP-OES analyzer. Elemental analyses were measured using EURO EA equipment. Particle size analysis of colloidal samples (concentration 1 wt %) was performed by dynamic light scattering (DLS) using a Malvern Zetasizer Nano ZS. Transmission electron microscopy (TEM) measurements were carried out on a JEOL Tecnai-G2, FEI, analyzer at 200 kV. The TEM sample was prepared using carbon-coated copper grids (300 mesh) and by drying a small droplet of the aqueous particle dispersion overnight in deionized and oxygen-free water (~5 μL) on it in an argon atmosphere. The oxidation states of metals were determined using an ESCALAB 250.

4.2. Synthesis of Hydroxyl Group-Functionalized Boron Nanoparticles ($B_m(OH)_n$). Boron nanoparticles were prepared according to the procedure reported in the literature.[16] Thus, a 5.0 mL toluene solution of $B(NCO)_3$ in a 100 mL high-vacuum flask equipped with a stirring bar was degassed three times and subsequently charged with highly pure hydrogen gas to reach its pressure of 1 atm. The reaction mixture was heated to 50 °C in the dark for 30 min. After cooling to room temperature, the flask was transferred to a glovebox, and the gases present in the flask were released

https://doi.org/10.1021/acsomega.1c05888
ACS Omega 2022, 7, 5864−5869

carefully. The resulting dark-brown solid was precipitated and collected by centrifugation, followed by washing with anhydrous toluene (2 × 5.0 mL) before being collected and dried inside the glovebox.

Functionalized boron nanoparticles ($B_m(OH)_n$) were prepared by a hydrolysis reaction with *in situ* generated brominated boron nanoparticles as shown in Figure 2a. A suspension solution with ~3.0 mg of freshly synthesized boron nanoparticles in 5.0 mL of anhydrous carbon disulfide was treated with 55.0 μL of bromine and stirred continuously for 10 h at room temperature. The resulting deep dark-brown solid was precipitated and washed with anhydrous toluene (2 × 5.0 mL). The resulting solid residue was suspended in 5.0 mL of distilled water and treated with 2.0 mL of 1.0 N sodium hydroxide solution and two drops of hydrogen peroxide solution (3% w/w) for 2 days. The reaction mixture was then neutralized with a 1.0 N hydrogen chloride aqueous solution to produce a dark-brown solid as a precipitate. The solid was collected by centrifugation, followed by washing with distilled water (2 × 5.0 mL) and acetone (2 × 3.0 mL) before being dried in the glovebox. The boron nanoparticles were analyzed using ^{1}H and ^{11}B NMR spectra, FT-IR spectra, ICP-OES, and TEM. The boron concentration was 98.77% (w/w) determined by ICP-MS measurement (m/n = 126.32). ^{1}H and ^{13}C NMR ($CDCl_3$, relative to $SiMe_4$; ppm): no absorptions of functional groups except deuterated solvents peaks. ^{11}B NMR (DMSO-d_6, relative to $BF_3{\cdot}OEt_2$; ppm): δ 30.15 (single, broad). FT-IR (film on KBr, cm^{-1}) 3447 (vs, br), 1637 (m, s), 1409 (s, s), 1195 (s, s), 1080 (s, br), 802 (s, br), 647 (s, s), 548 (s, s). The TEM, DLS, and XPS images of the product are shown in Figure 3.

4.3. Cytotoxicity Analysis. The Uppsala 87 malignant glioma (U87MG) cell lines, malignant melanoma A375 cell lines, KB human oral cancer cell lines, rat cortical neuron cell lines, and rat fibroblast-like synoviocyte (FLS) cell lines were used to test the cytotoxicity of the functionalized boron nanoparticles using the standard MTT method. The cells were treated with serial dilutions of the inhibitor (1000−3.906 μM, 1% DMSO, final) in complete reaction buffer and incubated for 96 h. The IC_{50} values of the functionalized boron nanoparticles ($B_m(OH)_n$) are greater than 1000 μM for all of the examined cell lines as shown in Figure 4.

4.4. Boron Uptake Assay. Briefly, 5.0 × 10^8 rat FLS cells or 3.5 × 10^7 U87MG cells were seeded and cultured at 37 °C with 5% CO_2 for 24 h before the culture medium was removed by suction. The culture medium containing 0.01 mM functionalized boron nanoparticles ($B_m(OH)_n$) was then added, and the cells were cultured for another 24 h under the same conditions. The culture medium was removed by suction, and the cells were washed three times with PBS and treated with trypsin to recover the cells. The number of cells recovered was counted, HNO_3 (2 N, 1.5 mL) was added, and the resulting mixture was heated at 80 °C for 12 h. After filtering with a membrane filter, the boron concentration was determined using ICP-OES. The results are as follows: hydroxyl boron nanoparticles ($B_m(OH)_n$), 201.53 (U87MG) and 147.64 (FLS) μg boron/10^7 cells.

4.5. *In Vitro P. falciparum* Growth Inhibition Assay. The asexual 3D7 strain of *P. falciparum* parasites was maintained *in vitro* in human O+ erythrocytes at 4% hematocrit in RPMI-1640 medium (Invitrogen, U.K.) supplemented with 2 mM L-glutamine, 25 mM HEPES, 2 g/L sodium bicarbonate, 5 g/L AlbuMAX I (Life Technologies), 0.37 mM hypoxanthine, and 40 mg/L gentamicin under a gas mixture of 5% O_2, 5% CO_2, and 90% N_2, at 37 °C. The parasite culture was synchronized every 3−4 days with 5% sorbitol and transferred into a fresh complete medium with uninfected erythrocytes.

The growth inhibition assay was conducted according to the literature with slight modifications.[25] In brief, synchronized ring-stage parasites at 1% parasitemia and 2% hematocrit were added to individual wells of a 96-well black plate, while nonparasitized erythrocytes at 2% hematocrit served as reference controls. The test compounds were prepared at a stock concentration of 1 M in DMSO, serially diluted in complete medium, and dispensed into duplicate test wells to yield final concentrations ranging from 0 to 1000 μM. The plates were incubated at 37 °C with a gassed environment of 5% O_2, 5% CO_2, and 90% N_2. Forty-eight hours later, SYBR Green I solution (0.2 μL of SYBR Green I/mL buffer solution consisting of 20 mM Tris 20, pH 7.5, 5 mM EDTA, 0.008% w/v saponin, and 0.08% v/v Triton X-100) was added to each well and mixed at 1000 rpm for 30 s using a microplate mixer. After 1 h of incubation in the dark at room temperature, the fluorescence signal was measured with a Spectramax M5 multimode microplate reader (Molecular Devices) with excitation and emission wavelength bands centered at 485 and 535 nm, respectively. The background reading from the wells of nonparasitized erythrocytes was subtracted to yield fluorescence counts for analysis. The SYBR Green I signals in drug-treated samples were normalized to the untreated control parasite samples in the same experiment, which were taken as 100%. Fifty percent inhibitory concentrations (IC_{50} values) with standard deviation (SD) were calculated from at least three experiments. Standard antimalarial drugs, pyrimethamine and chloroquine, were used as the positive antimalarial control. The results are shown in Figure 5.

4.6. Statistical Analysis. Statistical analysis and drawing graphs were carried out using Prism 9 for macOS version 9.02, GraphPad Software, LLC. The *in vitro* BNCT was carried out in triplicate. The values are the mean ± SEM from three independent experiments. The significance of the differences in survival rates was assessed by Student's *t* test.

■ ASSOCIATED CONTENT

Supporting Information

The Supporting Information is available free of charge at https://pubs.acs.org/doi/10.1021/acsomega.1c05888.

XPS survey scans of compound $B_m(OH)_n$ (PDF)

■ AUTHOR INFORMATION

Corresponding Authors

Yinghuai Zhu − *State Key Laboratory of Anti-Infective Drug Development (NO 2015DQ780357), Sunshine Lake Pharma Co., Ltd., Dongguan 523871, China;* orcid.org/0000-0001-7572-6867; Email: zhuyinghuai@hec.cn

Chairat Uthaipibull − *National Center for Genetic Engineering and Biotechnology (BIOTEC), National Science and Technology Development Agency (NSTDA), Pathum Thai 12120, Thailand;* Present Address: Thailand Center of Excellence for Life Sciences, Bangkok 10400, Thailand; Email: chairat.u@tcels.or.th

https://doi.org/10.1021/acsomega.1c05888
ACS Omega 2022, 7, 5864−5869

Authors

Parichat Prommana − *National Center for Genetic Engineering and Biotechnology (BIOTEC), National Science and Technology Development Agency (NSTDA), Pathum Thai 12120, Thailand*

Narayan S. Hosmane − *Department of Chemistry and Biochemistry, Northern Illinois University, DeKalb, Illinois 60115, United States;* orcid.org/0000-0002-6421-7546

Paolo Coghi − *School Pharmacy, Macau University of Science and Technology, Macau 999078, China*

Yingjun Zhang − *State Key Laboratory of Anti-Infective Drug Development (NO 2015DQ780357), Sunshine Lake Pharma Co., Ltd., Dongguan 523871, China*

Complete contact information is available at: https://pubs.acs.org/10.1021/acsomega.1c05888

Author Contributions

Y.Z. created the idea, designed and partially performed the experiments, and wrote the paper; P.P., C.U., and P.C. performed the experiments and reviewed the paper; and N.S.H. and Y.Z. reviewed the paper. All authors have read and agreed to the published version of the manuscript.

Notes

The authors declare no competing financial interest.

■ ACKNOWLEDGMENTS

This work was supported by the HEC Pharm Group in Dongguan City, Guangdong, China, and funded by the Science and Technology Development Fund, Macau SAR (file no. 0030/2018/A1).

■ REFERENCES

(1) https://www.cdc.gov/malaria/about/biology/index.html (accessed Aug 10, 2021).

(2) WHO. *World Malaria Report 2019*; World Health Organization: Geneva, Switzerland, 2019. https://www.who.int/publications/i/item/9789240015791.

(3) Woodley, C. M.; Amado, P. S. M.; Cristiano, M. L. S.; O'Neill, P. M. Artemisinin inspired synthetic endoperoxide drug candidates: Design, synthesis, and mechanism of action studies. *Med. Res. Rev.* **2021**, *41*, 3062−3095.

(4) Tarnchompoo, B.; Sirichaiwat, C.; Phupong, W.; Intaraudom, C.; Sirawaraporn, W.; Kamchonwongpaisan, S.; Vanichtanankul, J.; Thebtaranonth, Y.; Yuthavong, Y. Development of 2,4-diaminopyrimidines as antimalarials based on inhibition of the S108N and C59R +S108N mutants of dihydrofolate reductase from pyrimethamine-resistant *Plasmodium falciparum*. *J. Med. Chem.* **2002**, *45*, 1244−1252.

(5) *Report on Antimalarial Drug Efficacy, Resistance and Response: 10 Years of Surveillance (2010−2019)*; World Health Organization, 2020.

(6) Rasmussen, C.; Alonso, P.; Ringwald, P. Current and emerging strategies to combat antimalarial resistance. *Expert Rev. Anti-Infect. Ther.* **2021**, *17*, 1−20.

(7) Blasco, B.; Leroy, D.; Fidock, D. A. Antimalarial drug resistance: linking *Plasmodium falciparum* parasite biology to the clinic. *Nat. Med.* **2017**, *23*, 917−928.

(8) Coghi, P. S.; Zhu, Y.; Xie, H.; Hosmane, N. S.; Zhang, Y. Organoboron Compounds: Effective Antibacterial and Antiparasitic Agents. *Molecules* **2021**, *26*, No. 3309.

(9) Jacobs, R. T.; Plattner, J. J.; Keenan, M. Boron-based drugs as antiprotozoals. *Curr. Opin. Infect. Dis.* **2011**, *24*, 586−592.

(10) Anacor Pharmaceuticals. FDA Approves Anacor Pharmaceuticals' KERYDIN(Tavaborole) Topical Solution, 5% for the Treatment of Onychomycosis of the Toenails. Press Release, 8 July 2014.

(11) Hoy, S. M. Crisaborole ointment 2%: A review in mild to moderate atopic dermatitis. *Am. J. Clin. Dermatol.* **2017**, *18*, 837−843.

(12) Zhu, Y.; Wu, G.; Zhu, X.; Ma, Y.; Zhao, X.; Li, Y.; Yuan, Y.; Yang, J.; Yu, S.; Shao, F.; et al. Synthesis, in vitro and in vivo Biological Evaluation, and Comprehensive Understanding of Structure—Activity Relationships of Dipeptidyl Boronic Acid Proteasome Inhibitors Constructed from-Amino Acids. *J. Med. Chem.* **2010**, *53*, 8619−8626.

(13) Han, L.; Wen, Y.; Li, R.; Xu, B.; Ge, Z.; Wang, X.; Cheng, T.; Cui, J.; Li, R. Synthesis and biological activity of peptide proline-boronic acids as proteasome inhibitors. *Bioorg. Med. Chem.* **2017**, *25*, 4031−4044.

(14) Urbán, P.; Fernàndez-Busquets, X. Nanomedicine against malaria. *Curr. Med. Chem.* **2014**, *21*, 605−629.

(15) Borgheti-Cardoso, L. N.; Anselmo, M. S.; Lantero, E.; Lancelot, A.; Serrano, J. L.; Hernan-Ainsa, S.; Fernandez-Busquets, X.; Sierra, T. Promising nanomaterials in the fight against malaria. *J. Mater. Chem. B* **2020**, *8*, 9428−9448.

(16) Zhu, Y.; Hosmane, N. S. Liquid-Phase Synthesis of Boron Isocyanates: Precursors to Boron Nanoparticles. *Angew. Chem., Int. Ed.* **2018**, *57*, 14888−14890.

(17) Baber, R. A.; Norman, N. C.; Orpen, A. G.; Rossi, J. The solid-state structure of diboronic acid, $B_2(OH)_4$. *New J. Chem.* **2003**, *27*, 773−775.

(18) Agarwal, P. P. K.; Jensen, D.; Chen, C.-H.; Rioux, R. M.; Matsoukas, T. Surface-Functionalized Boron Nanoparticles with Reduced Oxide Content by Nonthermal Plasma Processing for Nanoenergetic Applications. *ACS Appl. Mater. Interfaces* **2021**, *13*, 6844−6853.

(19) Rohani, P.; Kim, S.; Swihart, M. T. Boron Nanoparticles for Room-Temperature Hydrogen Generation from Water. *Adv. Energy Mater.* **2016**, *6*, No. 1502550.

(20) Kirk, K. Membrane Transport in the Malaria-Infected Erythrocyte. *Physiol. Rev.* **2001**, *81*, 495−537.

(21) Prajapati, S. K. Alteration of the Red Blood Cell Membrane. In *Encyclopedia of Malaria*; Hommel, M.; Kremsner, P., Eds.; Springer: New York, NY, 2014.

(22) Hunter, P. Not boring at all. Boron is the new carbon in the quest for novel drug candidates. *EMBO Rep.* **2009**, *10*, 125−128.

(23) Fink, K.; Uchman, M. Boron cluster compounds as new chemical leads for antimicrobial therapy. *Coord. Chem. Rev.* **2021**, *431*, No. 213684.

(24) Armarego, W. L. F.; Perrin, D. D. *Purification of Laboratory Chemicals*, 4th ed.; Butterworth-Heinemann: Woburn, 2000.

(25) Moll, K.; Kaneko, A.; Scherf, A.; Wahlgren, M. *Methods in Malaria Research*, 6th ed.; EVIMalaR: Glasgow, U.K., 2013.